Journal of ELECTRONIC MATERIALS, Vol. 49, No. 9, 2020
https://doi.org/10.1007/s11664-020-08119-5

TOPICAL COLLECTION: 18TH CONFERENCE ON DEFECTS (DRIP XVIII)

Electrical Activity of Crystal Defects in Multicrystalline Si

A. MORETÓN,[1] M.M. JIMÉNEZ,[1] S. DADGOSTAR,[1] O. MARTÍNEZ,[1] M.A. GONZÁLEZ,[1] and J. JIMÉNEZ[1,2]

1.—GdS-Optronlab Group, Dept. Física de la Materia Condensada, Universidad de Valladolid, Paseo de Belén, 19, 47011 Valladolid, Spain. 2.—e-mail: jimenez@fmc.uva.es

Upgraded metallurgical-grade silicon solar cells with different ranges of efficiencies have been characterized by light-beam-induced current (LBIC) measurements. The interaction between grain boundaries and metallic impurities is studied for cells fabricated on wafers from different solidification heights of the ingot. A tight relation is observed between the electrical activity of the grain boundaries and the position of the wafer in the ingot, which is related to the impurity contamination. The presence of a large amount of metallic impurities enhances the electrical activity of the grain boundaries. The main features of the LBIC images are discussed in relation to the presence of metallic impurities.

Key words: Multicrystalline Si, grain boundaries, LBIC, impurity gettering

INTRODUCTION

Directionally solidified multicrystalline silicon (mc-Si) accounts for a large share of the photovoltaic market. The availability of low-cost feedstock permits a substantial reduction of solar cell production costs. However, the presence of metallic impurities in this solar-grade material reduces the carrier lifetime and photovoltaic efficiency. The reduction in efficiency is associated with various mechanisms, e.g., bulk recombination, surface recombination, optical losses, series resistance losses, and shunt losses.[1] Bulk recombination in mc-Si is mainly related to the presence of crystal defects, e.g., grain boundaries (GBs), small-angle grain boundaries (SAGBs), dislocations, and dislocation clusters. However, differences are observed in the electrical activity of these defects, and not all of them are effective traps for photogenerated carriers. The use of spatially resolved characterization techniques is crucial to reveal the electrical activity of GBs. Among such techniques, luminescence imaging, including both photoluminescence (PLi) and electroluminescence (ELi), is frequently used for full cell mapping.[2,3] The resulting images provide a quick view of the distribution of nonradiative recombination centers over the area of the cell; however, the spatial resolution does not enable detailed analysis of the electrical activity of crystal defects. Light-beam-induced current (LBIC) measurements permit one to map the spatial distribution of bulk recombination in solar cells with micrometric resolution. This allows the electrical activity of the GBs to be studied in detail, as the spatial resolution is better than that of ELi/PLi or lock-in thermography methods.[4] The electrical activity of GBs is a matter of controversy. It has been claimed that their activity is related to the presence of metallic impurities, as they are usually found in the highest concentration around GBs and dislocation clusters.[5] Understanding the interaction between defects and metallic impurities is a critical issue for mc-Si technology. Metallic impurities are mainly gettered by random-angle GBs (RAGBs),[6] and SAGBs, which are formed by a dense line of dislocations.[5,7]

We present herein a study of the electrical activity of extended defects in upgraded metallurgical-grade (UMG) mc-Si using high-spatial-resolution LBIC measurements. UMG mc-Si is of great interest for the photovoltaic industry as it provides cell efficiencies up to 20% at lower cost.[8] Also, it

(Received November 25, 2019; accepted March 25, 2020; published online April 9, 2020)

provides a useful way to study the interaction between defects and metallic impurities, because of its higher metallic content compared with the purified Si feedstock used in conventional mc-Si cells. The impurity concentration presents a gradient along the growth axis due to segregation. We study the electrical activity of defects along the growth axis using cells fabricated on wafers cut from different solidification heights of the ingot, which exhibit similar grain structure but different concentrations of impurities because of the concentration gradient along the growth axis. It has been claimed that the recombination activity of GBs depends on the position of the wafer in the ingot, which is associated with the level of contamination.[9]

EXPERIMENTAL PROCEDURES

LBIC measurements were carried out using a homemade system with an 853-nm laser as the excitation source, for which the penetration depth in Si is ~13 μm.[10] A beam splitter divides the output beam of the laser (10 mW) into two beams. One of them is used to measure variations in the output power using a photodiode, while the other is directed into a trinocular microscope which focuses the laser onto the solar cell. The measurements were carried out using 20× and 50× objectives. LBIC scanning was achieved by moving the sample on an *x–y–z* motorized translation stage (Prior Scientific) allowing step sizes as small as 1 μm. The spatial resolution of LBIC images is determined by the objective and step size, and under selected conditions one can reach micrometric spatial resolution. A Si charge-coupled device (CCD) camera coupled to the top ocular of the microscope was used to collect the light reflected by the sample and drive an autofocus system. The locally generated photocurrent was recorded using an electrometer (Keithley Instruments). Data acquisition and hardware control were implemented in LabVIEW. For more details see Ref. 11.

The solar cells were supplied by Silicio Ferrosolar (Arteixo, Spain). The cell fabrication followed the standard technological stages, including gettering and hydrogenation. The cells were fabricated on wafers cut from different heights of the ingot. The cell efficiencies varied from ~ 16% for the wafers from the ingot bottom to ~17.8% for the wafers from the middle of the ingot.

RESULTS AND DISCUSSION

Figure 1 shows an LBIC image (1a) and reflected light image (1b) of a standard cell fabricated on conventional directionally solidified mc-Si. The regions with different reflectivity are related to variations in the surface texture, which depends on the grain orientation; this reveals the grains and GBs, while small-tilt-angle grain boundaries are barely observable in the reflected image. The LBIC image reveals that most of the GBs observed in the reflected light image present weak electrical activity, while intragrain defects (SAGBs and dislocation clusters) appear to be electrically active, even if not revealed in the reflected light image. The LBIC image is corrected to compensate for reflectivity losses.

LBIC images of three sister cells are shown in Fig. 2, revealing that the electrical activity of the defects progressively reduced from the bottom to top as the concentration of impurities reduced due to segregation; a concomitant increase of the cell efficiency from 16% to 17.8% is also observed. The recombination activity of the GBs is related to the density of dislocations in the boundary plane, which is associated with the type of boundary,[12] and the impurity contamination.[13]

The same defect structures were mapped by LBIC for the three samples, which permits comparative analysis between them to evaluate the influence of the impurity contamination. Cell A exhibited dark contrast for coincident site lattice (CSL) GBs and random-angle GBs (RAGBs). However, this contrast was substantially smoothed for cell B, especially for the GBs, although the main contrast features seen for cell A were still observed for cell B. Cell C presented some dark-contrast RAGBs, but most of the GBs and RAGBs revealed for cell A appeared to be electrically inactive. The electrical activity of the defects was related to the impurity contamination and the structure of the defect itself. Transition-metal impurities are usually present in this kind of material at concentrations close to 10^{14} cm^{-3} to 10^{16} cm^{-3},[6] decreasing in the middle of the ingot down to ~ 10^{12}–10^{13} cm^{-3} with respect to the top and bottom zones, which are more highly contaminated. Cell C came from the middle of the ingot, while cells B and A were obtained from closer to the bottom, thus they contain a higher concentration of residual impurities. From these results, it appears that the background impurity concentration plays a major role in the electrical activity of the defects. The activity of the GBs is related to the density of dislocations in the boundary plane, while their decoration with impurities makes them electrically active.[12]

Cell A was obtained from closest to the bottom of the ingot, thus it was the one with the highest concentration of impurities. A bright-contrast halo was observed around the high-contrast dark lines (GBs and RAGBs), corresponding to an impurity-denuded zone created by gettering of impurities by GBs. It is worth noting that, in the region presenting a higher concentration of boundaries (circle area in Fig. 3, cell A), the gettering of impurities by the boundaries leaves a large area with bright LBIC contrast, corresponding to enhanced internal quantum efficiency (IQE). This is consistent with the strategy of decreasing the grain size using a structure with RAGBs to obtain high-performance multicrystalline Si (HPmc-Si), which results in

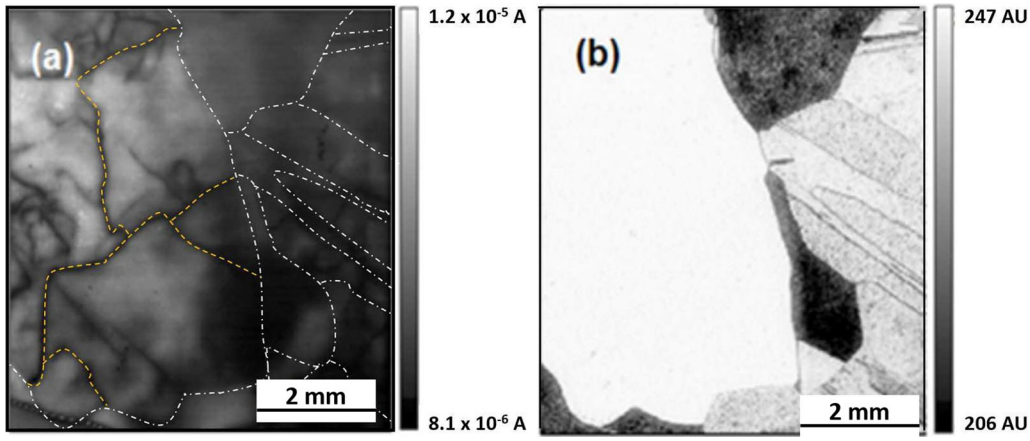

Fig. 1. (a) LBIC image (853 nm, 20× objective) and (b) reflected light image of a conventional cell. Dotted white lines highlight GBs, while dotted yellow lines highlight some electrically active subgrain boundaries revealed by LBIC but not seen in the reflected light image (Color figure online).

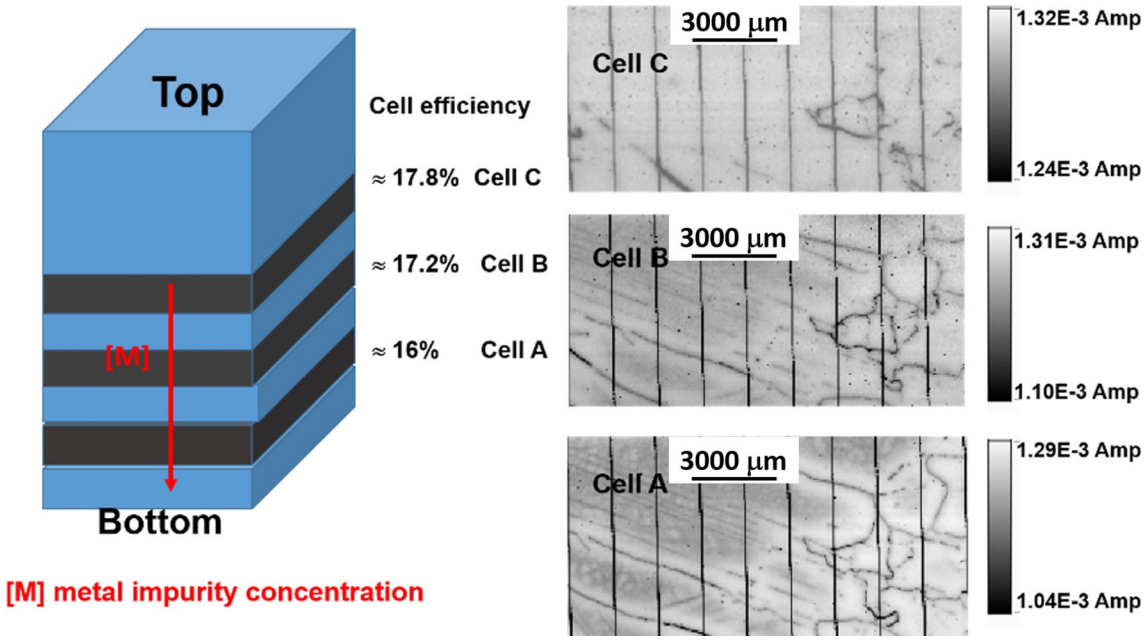

Fig. 2. Schematic showing the location of the UMG cells along the ingot, and LBIC images of three sister cells from three regions of the ingot from the bottom to middle (A, B, and C), showing a similar defect distribution but different levels of electrical activity.

enhanced cell efficiency.[14] The average LBIC current in this region was higher than that measured in large grains, despite the carrier trapping by the boundaries. In the middle of large grains, inhomogeneous soft contrast forming a cellular-like structure was observed, associated with an inhomogeneous impurity distribution inside the grains (Fig. 4a). This kind of distribution was not observed for all grains, which suggests that it could be associated with the grain structure and orientation, resulting in the inhomogeneous distribution of impurities. Therefore, dense arrays of RAGBs forming small grains should enable an increase in the internal quantum efficiency (IQE) as compared with large grains, at least for highly contaminated material.

Dark boundaries around which the bright halo corresponding to impurity depletion is less marked were also observed (Fig. 3a, arrow indicating a GB with a tenuous halo). This suggests that the gettering of impurities is less efficient, even if some of them present dark contrast; therefore, the boundary structure itself may play a main role in impurity gettering. The largest bright halo, and therefore the most efficient impurity gettering, is observed for RAGBs. Note that the LBIC profile around the boundaries does not only reflect the capture of minority carriers by the boundary but also is correlated with the impurity distribution around the boundaries, which reduces the effective carrier lifetime and thereby the diffusion length, which is substantially shortened around the defects.[15]

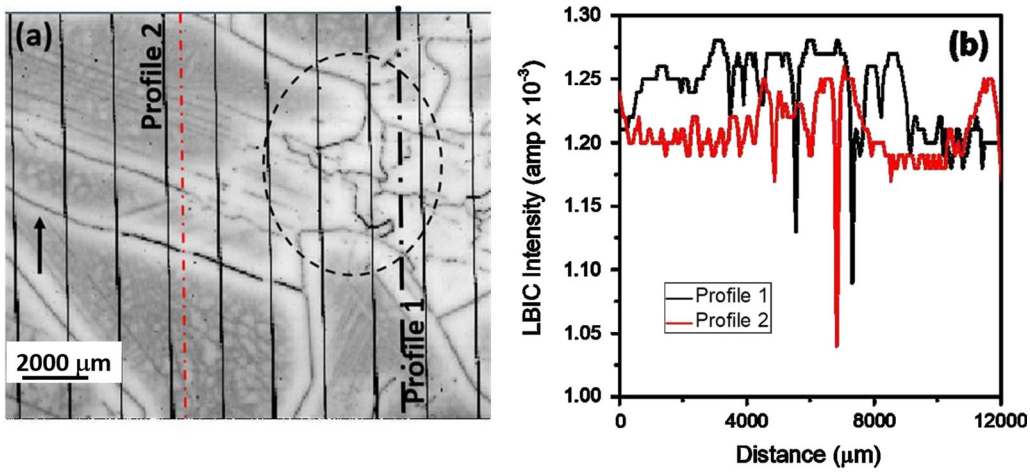

Fig. 3. The region inside the circle with a high concentration of RAGBs presents a higher LBIC signal than the large grains, due to gettering of impurities by RAGBs. The average LBIC intensity is enhanced in the encircled region in spite of the recombination activity of the RAGBs; see the LBIC profiles in the right panel (b), where a higher LBIC intensity is recorded along profile 1. Therefore, dense arrays of RAGBs forming small grains should allow an increase in the internal quantum efficiency (IQE) as compared with large grains.

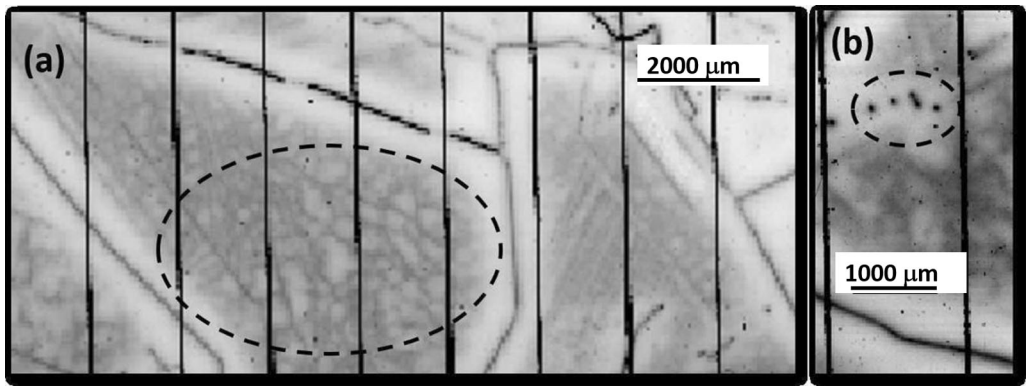

Fig. 4. (a) LBIC cellular-like distribution inside a large grain. (b) LBIC dark spots surrounded by an impurity-denuded halo (cell A).

Generally, the contrast profiles at each side of the boundaries are different, which is related to the different distribution of impurities on each side of the GB. Dark-contrast spots were also observed inside the large grains, surrounded by a denuded halo. These dark spots seem to consist of dislocation clusters, which are very efficient at gettering impurities (Fig. 4b). The dark contrast of the GBs is not homogeneous but rather presents different levels of contrast along the boundaries, which may be related to their ability to capture impurities.

Cell B was obtained from closer to the middle of the ingot, and the contrast around the boundaries was greatly smoothed with respect to cell A, the GBs being much less visible in the LBIC images (Fig. 2). Also, the impurity distribution inside the grains was different, and the cellular-like structure observed for cell A was no longer observed; furthermore, the denuded halo around the boundaries was significantly softened with respect to cell A.

Finally, in cell C, most of the dark-contrast features disappeared, concomitantly with the lower concentration of impurities in this part of the ingot, showing that decoration with impurities plays a crucial role in the electrical activity of the crystal defects.

LBIC contrast profiles along equivalent lines for the three cells are shown in Fig. 5. A significant decrease of the LBIC contrast is observed from cell A to cell C. Note also how the boundaries are slightly different in cells A and B, indicating that the walls of the grains are not parallel to the ingot axis but are tilted, and subgrains that change the defect structure along the ingot are formed. The LBIC contrast of the three cells reveals that passivation of GBs can only be achieved below a certain threshold concentration of impurities. Cell C is close to this threshold, as many of the GBs are not electrically active; meanwhile, the passivation is not effective for the case of a high concentration of

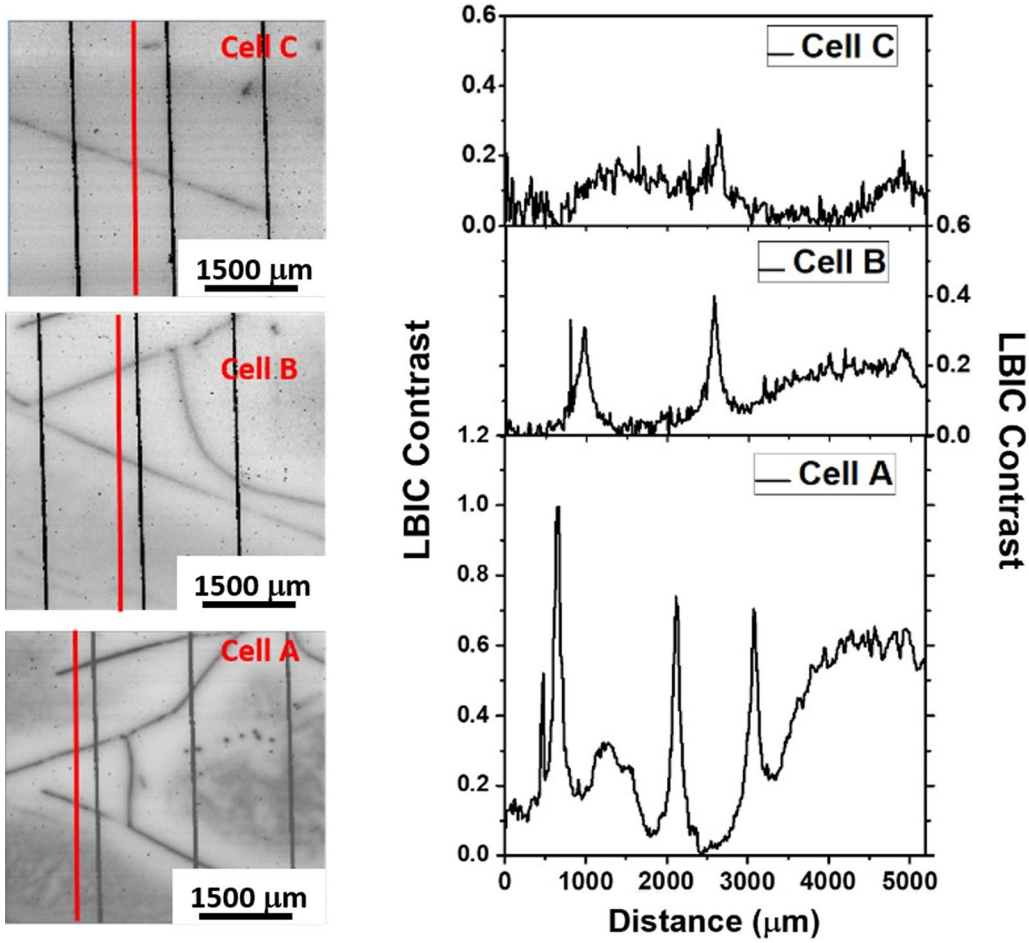

Fig. 5. LBIC contrast along lines drawn in the LBIC images, showing a progressive reduction of contrast from cell A to C as the electrical activity of GBs decreases because of the lower concentration of impurities.

impurities (cell A) and to a minor extent for cell B, in which most of the GBs are still electrically active.

CONCLUSIONS

We studied the electrical activity of UMG mc-Si solar cells by LBIC mapping. The use of sister cells permitted direct comparison of the electrical activity of GBs for different levels of impurity contamination. The electrical activity of the GBs appeared to be tightly related to the presence of impurities. RAGBs acted as getter centers for impurities. Denuded zones around the GBs, especially RAGBs, were observed in cells fabricated on wafers obtained from the bottom of the ingot, which turn out to be highly contaminated. The LBIC contrast softened progressively as the wafer location approached the middle of the ingot, where the impurity concentration is substantially reduced. The use of dense arrays of RAGBs permits an increase in the IQE of this material.

ACKNOWLEDGMENTS

This work was supported by Project VA283P18 (Junta de Castilla y León) and Project ENE2017-89561-C4-3-R (Spanish Ministry of Economics and Competitiveness), and the European Fund for Regional Development (FEDER).

REFERENCES

1. B. Michl, M. Padilla, I. Geisemeyer, S.T. Haag, F. Schindler, M.C. Schubert, and W. Warta, *IEEE J. Photovolt.* 4, 1502 (2014).
2. T. Trupke, R.A. Bardos, M.C. Schubert, and W. Warta, *Appl. Phys. Lett.* 89, 044107 (2006).
3. O. Breitenstein, J. Bauer, T. Trupke, and R.A. Bardos, *Prog. Photovol. Res. Appl. Prog.* 16, 325 (2008).
4. M. Padilla, B. Michl, B. Thaidigsmann, W. Warta, and M.C. Schubert, *Sol. Energy Mater. Sol. Cells* 120, 282 (2014).
5. T. Buonassisi, A.A. Istratov, M.D. Pickett, M.A. Marcus, T.F. Ciszek, and E.R. Weber, *Appl. Phys. Lett.* 89, 042102 (2006).
6. S. Castellanos, K.E. Ekstrom, A. Autruffe, M.A. Jensen, A.E. Morishige, J. Hofstetter, P. Yen, B. Lai, G. Stokkan, C. Del Canizo, and T. Buonassisi, *IEEE J. Photovolt.* 6, 632 (2016).
7. K. Adamczyk, R. Søndenå, G. Stokkan, E. Looney, M. Jensen, B. Lai, M. Rinio, and M. Di Sabatino, *J. Appl. Phys.* 123, 055705 (2018).
8. P. Zheng, F.E. Rougieux, X. Zhang, J. Degoulange, R. Einhaus, P. Rivat, and D.H. MacDonald, *IEEE J. Photovolt.* 7, 58 (2017).
9. J. Chen, T. Sekiguchi, S. Nara, and D. Yang, *J. Phys.: Condens. Matter* 16, S211 (2004).
10. D.E. Aspnes and A.A. Studna, *Phys. Rev. B* 27, 985 (1983).
11. B. Moralejo, M.A. González, J. Jiménez, V. Parra, O. Martínez, J. Gutiérrez, and O. Charro, *J. Electron. Mater.* 39, 663 (2010).

12. W. Seifert, G. Morgenstern, and M. Kittler, *Semicond. Sci. Technol.* 8, 1687 (1993).
13. J. Chen, D. Yang, Z. Xi, and T. Sekiguchi, *J. Appl. Phys.* 97, 033701 (2005).
14. C.W. Lan, A. Lan, C.F. Yang, H.P. Hsu, M. Yang, A. Yu, B. Hsu, W.C. Hsu, and A. Yang, *J. Cryst. Growth* 468, 17 (2017).
15. L.A. Sánchez, A. Moretón, M. Guada, S. Rodríguez-Conde, O. Martínez, and J. Jiménez, *MRS Adv.* 3, 3359 (2018).